Analysis of ageing inhomogeneities in lithium-ion battery systems

Sebastian Paul [a],[*], Christian Diegelmann [a], Herbert Kabza [b], Werner Tillmetz [c]

[a] BMW Peugeot Citroën Electrification GmbH, Taunusstraße 41, 80807 München, Germany
[b] Ulm University, Institute of Energy Conversion and Storage, Albert-Einstein-Allee 47, 89081 Ulm, Germany
[c] Zentrum für Sonnenenergie- und Wasserstoff-Forschung Baden-Wrttemberg, Helmholtzstraße 8, 89081 Ulm, Germany

HIGHLIGHTS

► A thermal-electric-ageing-model for a battery system is introduced.
► Analysis of ageing inhomogeneities in lithium ion battery systems.
► Consideration of cell-to-cell variation regarding capacity loss.
► Consideration of temperature and state of charge differences within the storage system.
► Verification by measurements regarding cycle life in a storage system.

ARTICLE INFO

ABSTRACT

In this article, a new simulative approach that can determine ageing inhomogeneities in lithium-ion battery systems is outlined. The proposed method is based on a thermal electric ageing model of an entire battery system and the Monte Carlo Method. This method considers temperature inhomogeneities caused by active cooling within the battery system as well as cell spread and ageing spread caused by tolerances in the cell production. Each cell in the battery system model is represented by its own thermal electric cell model, having an initial capacity, initial internal resistance, ageing rate and thermal connection to the cooling system. In the experimental part of this research work, a battery system consisting of 96 lithium-ion cells based on the LiFePO4-technology was tested to investigate the capacity fade during a cycle life test. The results show that discrepancies in cells ageing within the battery system are a consequence of cell-to-cell spread and different loading of the cells, caused by temperature and SoC inhomogeneities within the battery system. Furthermore, the article will evince the gain of accuracy by using a battery system instead of a previous single cell approach for life prediction.

1. Introduction

Lithium-ion batteries are the most promising solution for energy storage system in automotive application, due to their high energy density and power density. The durability of battery systems in automotive large-scale production is one of the most challenging topics in the development of electrified vehicles (e.g. hybrid electric vehicles). A failure of the battery system is considered to occur when the energy or the power is reduced to a certain value. In many applications this value is considered 80% of the begin of life (BOL) performance [5]. The degradation of a lithium-ion battery, namely capacity loss and impedance increase, has been studied intensively

during the last few years. The main research efforts regarding cell ageing were dedicated to investigate the influence of different cycling and storage condition on battery behaviour. There are two different approaches to model ageing of lithium-ion batteries. The first one is based on a first principle method and considers electrochemical and physical processes within the cells. This approach is suitable to investigate the different ageing mechanisms in cells (e.g. degradation on the electrodes, active material loss) [2,10,11,13]. The second method is an empirical approach to predict capacity fade or resistance increase by fitting experimental data [1,9,12]. The previous mentioned approaches are focused on the investigation of single cell behaviour. In order to investigate the performance of an entire battery pack, [6] pointed out the influence of cell-to-cell variation (e.g. resistance and initial capacity). They demonstrated that the capacity of battery systems, consisting of a various number of cells in series connection, is determined by the weakest cell within the system. Thus, the lifetime of the battery system is

* Corresponding author.
E-mail addresses: Sebastian.Paul@bpc-electrification.com, sebastian_paul84@gmx.de (S. Paul), Christian.Diegelmann@bpc-electrification.com (C. Diegelmann).

specified by the lifetime of the weakest cell. Ref. [4] introduced a simulative approach to estimate the lifetime of lithium-ion batteries in plug-in hybrid electric vehicles (PHEV). These and other investigations regarding lifetime prediction of battery systems neglect thermal and electric inhomogeneities within the battery pack and cell-to-cell variation of ageing behaviour. They simply scale the behaviour of a single cell to the entire system. In order to investigate ageing inhomogeneities in a lithium-ion battery system of a hybrid electric vehicle, a new simulative approach is outlined. The proposed method is based on a 1D thermal electric model of an entire battery system, coupled with an empirical ageing model and the Monte Carlo Method to consider cell-to-cell variation (e.g. capacity, ageing rate) and inhomogeneities within the battery system (e.g. temperature, SoC).

2. Simulation

Fig. 1 shows the schematic structure of the proposed battery system model. The model is composed by 96 single cell models. Each cell model is represented by three sub-models namely, electrical, thermal and ageing model.

2.1. Single cell model

The cell model is represented by the combination of an impedance based equivalent circuit model (ECM) and a thermal model including heat generation and heat dissipation. Different ECM approaches used in Li-ion cell simulations are reviewed by Ref. [3]. The ECM approach for the electrical modelling was chosen in order to meet both, manageable computing complexity and necessary accuracy. The chosen ECM for this investigation consists of a serial resistance and two RC-circuits in series connection. All parts of this model are considered as temperature-, SoC- and current direction dependent. The model is calibrated for a cylindral 4.4 Ah lithium-ion cell based on a LiFePO4 chemistry. In Fig. 2, the used equivalent circuit diagram is presented. The heat generation model considers Joule heat and neglects reversible heat due to the application in a HEV with a net reversible heat effect near zero [14]. The Joule heat results directly from the ohmic losses of the cell. They can be calculated from the equivalent circuit model. In order to consider temperature dependences in cells electric behaviour it is mandatory to co-simulate the thermal and the electrical model [8]. The thermal model of the lithium-ion battery is based on a validated 3D spatialized thermal cell model, which is proposed by Ref. [7]. In order to meet both high accuracy and manageable computing time,

there are simplifications necessary. In Fig. 3, the chosen simplified thermal 1D-model is outlined. The model consists of 5 thermal masses, which are a representation for the jelly roll core, jelly roll, terminal, CAN and cooler. The thermal masses are connected through thermal resistances. In order to consider heat dissipation, the cooler is connected to two heat sinks, coolant and environment. The heat generation is applied at the jelly rolls thermal masses. The jelly roll is divided in two separate thermal masses in order to consider the temperature gradients within the cell due to active cooling. The thermal masses and resistances of the proposed simplified thermal model were determined by a fitting algorithm.

The ageing model of the lithium-ion battery is divided in a calendar and a cycle ageing model. Both models are based on an empirical approach. The calendar ageing model is temperature (T), time (t) and SoC dependent and is determined by an Arrhenius Law approach (Formula (1)). The cycle ageing model is a weighted energy throughput (EN) model. The weight function is determined by SoC, temperature, charge and discharge current (Formula (2)). The chosen cell ageing model is provided by the cell manufacturer and will not be focus of this work. It is further considered as being a tool to analyse the mean ageing of the used lithium ion cells. The model will be adapted in order to analyse the ageing spread within the battery system.

$$C_{loss,cal} = A \cdot \exp\left(\frac{-E_A}{R \cdot T}\right) \cdot t^B \cdot SoC^C \tag{1}$$

$$C_{loss,cycl} = f(SoC, T, C) \cdot EN^D \tag{2}$$

2.2. Battery system model

The focus of this work is a battery system consisting of 96 cells in series connection. In order to investigate inhomogeneous cell behaviour within the battery system it is necessary to consider all factors which are leading to different cell loads. The main influence on different cell loads within the battery system is active cooling. The storage system of this investigation is cooled by direct AC-cooling consisting of two parallel cooling strands (Fig. 4). As inherent to their functional principle, this cooling system has a temperature difference up to 15 K. This temperature difference is due to the phase transition of the coolant, which is depending on ambient temperature, pressure and heat dissipation. Due to the pressure dependency of the vaporization each cell in the storage system is cooled by a different coolant temperature (Fig. 5).
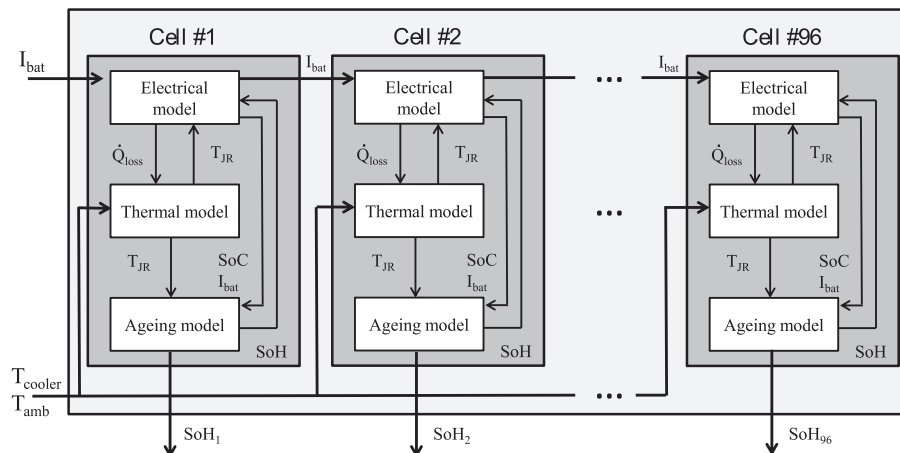

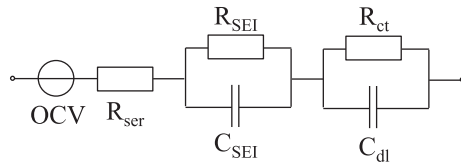**Fig. 1.** Schematic structure of the battery system model.

Fig. 2. Schematic of the equivalent circuit model.

In order to simulate the coolant temperature, the cooling system is represented by a simplified model. This considers the coolant as a control volume with a cooling capability, which depends on the position in the cooling system, ambient temperature and waste heat of the storage system. The waste heat of each cell is added to the coolant control volume in order of cell position in the cooling circuit. With this approach it is possible to calculate the residual cooling capability at each point in the circuit and the point of overheating. At this point in the cooling circuit the coolant is fully vaporized and the cooling capability drops drastically. Thus, the connected cells are not able to dissipate all of their waste heat to the cooler.

Fig. 4 shows that there are two different kinds of cells in the storage system, the ones with a direct connection to storage system casing and the ones which are at the inner part of the storage system. Thus, there are two different cooling rates of the cells to the environment. Each cell in the storage system can be initialized with different cell capacity and internal resistance in order to consider cell-to-cell variation.

2.3. Cell-to-cell variation

In a storage system consisting of a various number of cells, the cell-to-cell variation has a major influence on battery system lifetime. Fig. 6 shows the distribution of the initial cell capacity of over 20 000 cells. The distribution fits a normal distribution with a deviation of 1.3% of the nominal capacity. Fig. 7 shows the distribution of the cells direct current internal resistance (DCR) at the begin of life, with a deviation of 5.8% of the nominal DCR.

In addition to the initial cell-to-cell variation there is an ageing dependent spread of capacity and internal resistance. In order to analyse the influence of cell-to-cell variation on the battery lifetime regarding capacity degradation, the internal resistance rise is

assumed to be equal at each cell. The ageing dependent spread of the cell capacities is divided in two parts − calendar life and cycle life spread. These spreads are due to production tolerances. Thus, even if the cell load is identical, the cells age slightly different. The ageing spread is assumed to follow a normal distribution, due to its production process related statistical behaviour. The mean value of the distribution is represented by the previous mentioned ageing models (Formula (1) and (2)), which describes the mean ageing behaviour. The basis for these ageing models are various numbers of cell ageing measurements. These measurements were conducted with various numbers of cells. The deviation of the ageing spread can be obtained from the same test data. It seems that there is a different deviation of the ageing spread at each point of life. Up to now, there is no indicator of a correlation between calendar and cycle ageing behaviour. Thus, the dependence is assumed to be random. The Monte Carlo Method (MCM) is used to combine the calendar and cycle ageing for each cell separately. Thus, every cell has a different ageing behaviour in order to consider ageing spread between the cells. The combination of calendar and cycle ageing is shown in Fig. 8. The two distributions (calendar, cycle ageing) are divided in N, M identical segments (even-numbered). In order to combine these distributions, the MCM is used to determine a segment number n ($n \in N$) and m ($m \in M$) for each cell separately. The deviation of the ageing distributions changes during the lifetime. In order to consider that a cell with a high ageing rate will not become a cell with a low ageing rate, the segment number of each cell remains unchanged during one simulation loop. The simulation ends if the resulting capacity distribution converges.

Fig. 9 illustrates the used methodology. The simulation starts with the setup of the initial capacities and internal resistances for all cells. These values were conducted by a begin of test characterization of the storage system. Afterwards the segment numbers n and m for the calendar and cycle ageing distribution were determined by using MCM for each cell separately. These numbers were set random according to a normal distribution (see Fig. 9). The mean values of these distributions are at $n = N/2$ respectively $m = M/2$. If one cell is setup with $n = N/2$ and $m = M/2$ they will behave exactly like the mean cell. Formula (3) illustrates the capacity loss of the cells in the storage system. It is always a part of the mean ageing behaviour and a part of the ageing deviation. The ageing deviation can also be negative in order to consider cells with a lower ageing rate than the mean cell.

$$C_{\text{loss}}(\text{cell } x) = \overbrace{\left[C_{\text{loss,cal,mean},x} + C_{\text{loss,cal,dev},x} \right]}^{C_{\text{loss,cal},x}} + \overbrace{\left[C_{\text{loss,cycl,mean},x} + C_{\text{loss,cycl,dev},x} \right]}^{C_{\text{loss,cycl},x}} \tag{3}$$
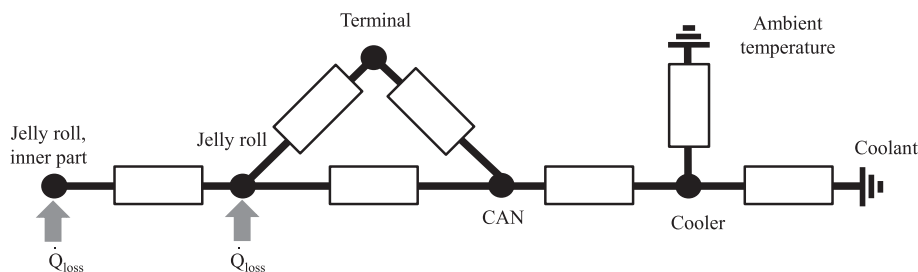

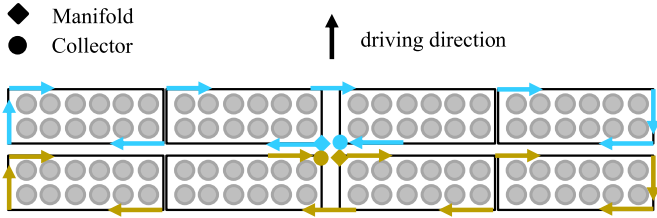**Fig. 3.** Schematic of the simplified 1D thermal model of a single cell.

Fig. 4. Storage system with an illustration of the two parallel cooling circuits (blue: cooling strand 1, yellow: cooling strand 2). (For interpretation of the references to colour in this figure legend, the reader is referred to the web version of this article.)
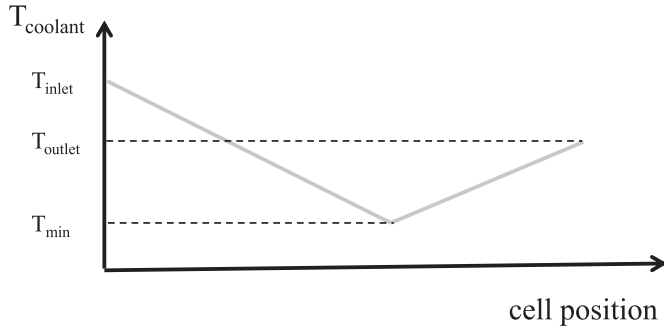

Fig. 5. Schematic temperature gradient in AC-cooling systems.

The mean ageing behaviour is represented by the ageing models in Formula (1) and (2). The deviation part of the ageing can be calculated by the following equations:

$$C_{loss,cal,dev} = \left(n - \frac{N}{2}\right) \cdot \sigma_{cal}(t, T, SoC) \quad (4)$$

$$C_{loss,cycl,dev} = \left(m - \frac{M}{2}\right) \cdot \sigma_{cycl}(EN) \quad (5)$$

By using Equations (1)–(5) the capacity loss for a cell x in the storage system is calculated with the Equation (6). In order to consider different cell loads due to thermal inhomogeneities within the storage system, the capacity loss of each cell is calculated with their actual temperature, SoC, current rate, energy throughput and ageing deviation.

$$
\begin{aligned}
C_{loss}(\text{cell } x) = &\left[A \cdot \exp\left(\frac{-E_A}{R \cdot T_x}\right) \cdot t^B \cdot SoC_x^C \right.\\
&\left. + \left(n_x - \frac{N}{2}\right) \cdot \sigma_{cal}(t, T_x, SoC_x)\right] \\
&+ \left[f(SoC_x, T_x, C) \cdot EN_x^D + \left(m_x - \frac{M}{2}\right) \cdot \sigma_{cycl}(EN_x)\right]
\end{aligned}
$$
$$(6)$$

At the end of one simulation loop the capacity distribution for all cells in the storage system is calculated. Afterwards the next simulation loop starts with a new setup of n and m. The simulation ends if the capacity distribution at the end of the test converges. It is not possible to predict the actual capacities for all 96 cells. This approach calculates a probability density of the cell capacities within the battery system, by summation of 96 single cell probabilities.

3. Results

A storage system consisting of 96 lithium-ion batteries was tested to investigate the ageing inhomogeneities within a battery system. By using a customer's driving profile for a hybrid electric vehicle a realistic ageing behaviour was achieved. Fig. 10 shows the current profile and the SoC development of this 2 h highway cycle. The cycle starts with a SoC of approx. 50% and ends with 40%. Thus, there is a short charging period at the end of each cycle necessary in order to achieve similar test conditions for all cycles.

Each cycle has an energy throughput of 20.9 kWh (approx. 0.21 kWh per cell). They were repeated in a test chamber with an ambient temperature of 24 °C. In order to keep the cells temperature at a moderate level, during this heavy duty cycle, the direct AC-cooling of the storage system was active. The cooling is
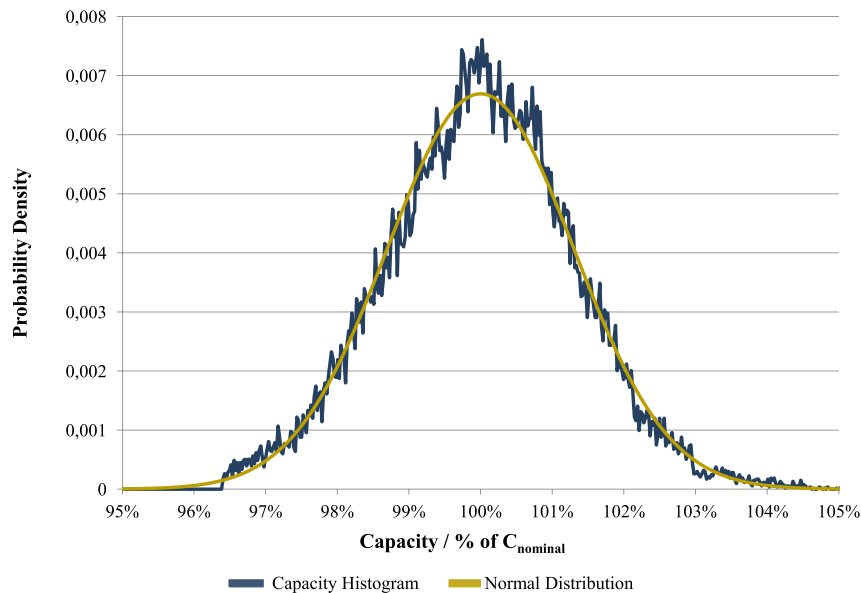

Fig. 6. Distribution cell capacity at begin of life ($\sigma = 1.3\%$ of nominal capacity, over 20 000 cells measured).
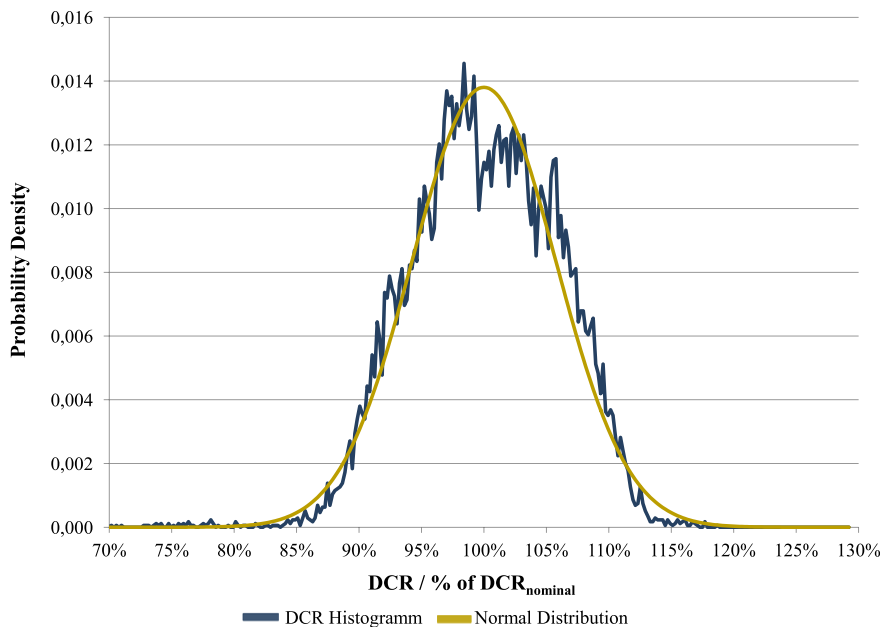
Fig. 7. Distribution DCR at begin of life ($\sigma = 5.8\%$ of nominal DCR, over 20 000 cells measured).
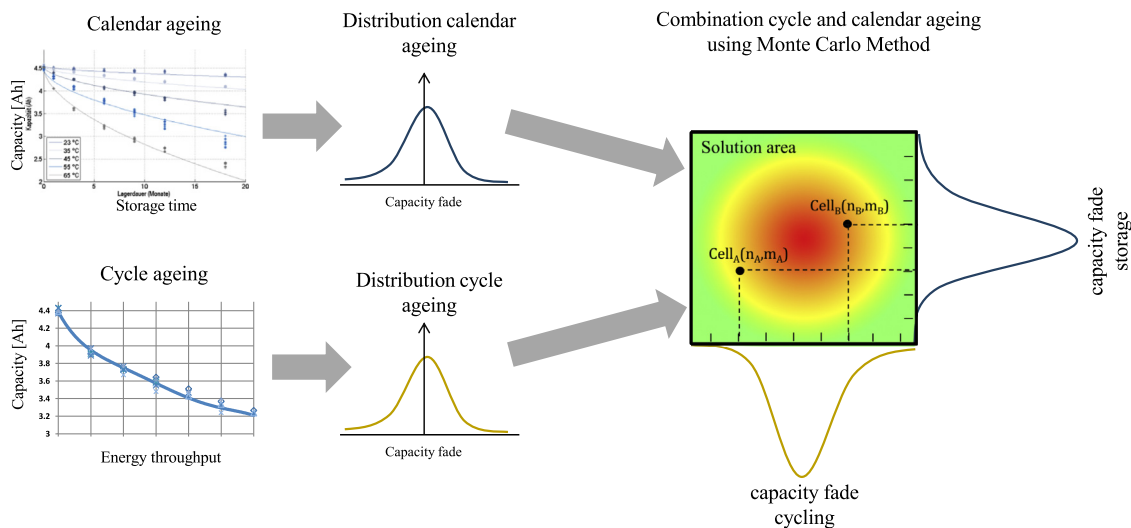

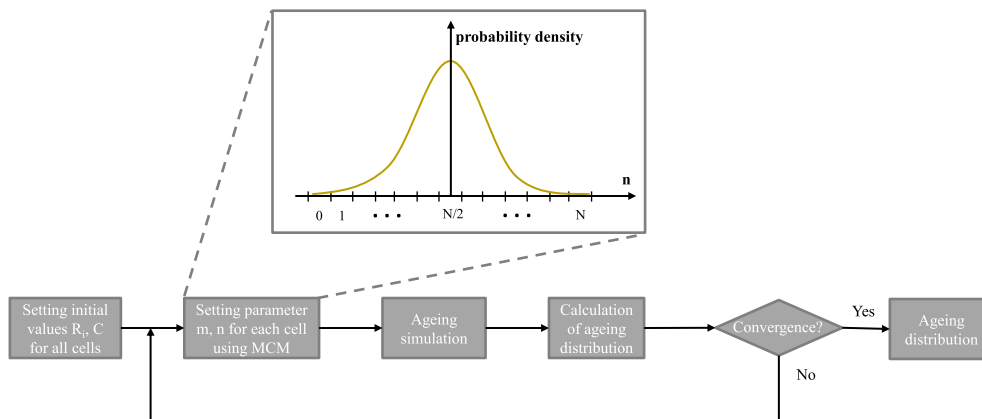**Fig. 8.** Combination of cycle and calendar ageing using MCM.

Fig. 9. Flowchart of the proposed methodology including one example of determining segment number n using MCM.
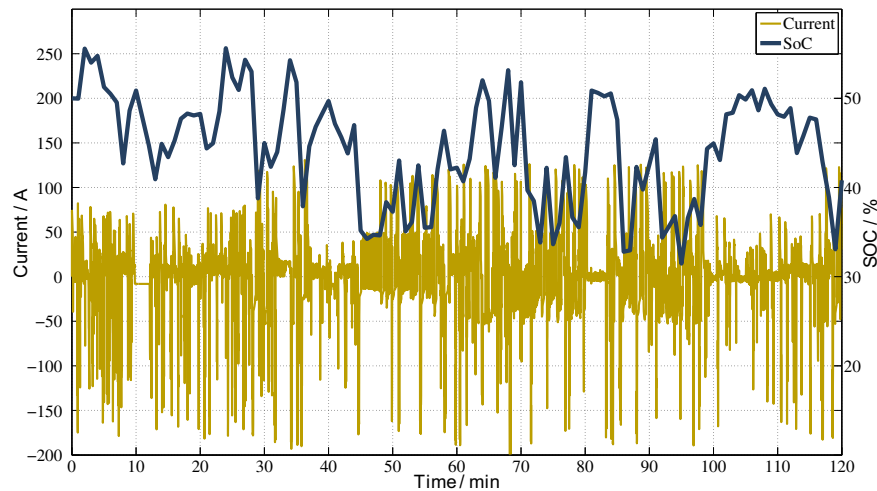
Fig. 10. Simulated current profile and SoC development of the 2 h cycle.

controlled by the temperature of the hottest cell within the system. The cooling thresholds were set to 32 °C (start cooling) and 28 °C (stop cooling).

Due to the different cell resistances shown in Fig. 11 and the temperature gradient within the cooling system, there is a temperature difference between the cells during cycling. Fig. 12 shows the temperature of the hottest and the coldest cell in the storage system during the 2 h driving cycle. The cells start with an identical temperature of 24 °C. Right after the beginning the temperatures diverged. There is a temperature difference of at least 4 K up to 7 K during the cycle. Since the temperature has a major influence on battery lifetime, the cells ageing rates within the storage system differs. Different cell capacities lead to different SoCs during cycling (Fig. 13). The SoC difference increases with higher capacity spread within the battery system.

Fig. 14 shows the development of cell capacities within the battery system during testing. The initial capacity spread of approximately 200 mAh decreases during the first 20 kWh to 100 mAh. It seems that the cells with a higher initial capacity are showing a higher initial ageing. After this initial ageing the capacity

spread increases up to 500 mAh at the end of testing. After 40 kWh one cell shows a significant higher ageing rate than the other ones. After this point, this cell limits the battery system capacity. There is a higher initial ageing rate during the first 40 kWh energy throughput followed by a region with a lower ageing rate. It seems there is no significant correlation between initial capacity and ageing rate. A comparison of cell capacities at begin of life and end of test is shown in Fig. 15. The average capacity loss is approximately 18%. There is an ageing spread between the cells from 14% at the best cell up to over 25% at the worst cell. This spread is due to different cell loadings according to different thermal conditions and cell-to-cell variation.

In order to demonstrate the outlined simulative approach, the ageing of this storage system was simulated, according to the test conditions. The model was initialized with the capacities and internal resistances for each cell, according to their position in the storage system. Fig. 16 shows the simulation results after 10 000 trails compared to the measured cumulated capacity distribution. The results after 45 kWh of cycling show a good accordance regarding worst cell behaviour and shape of the capacity
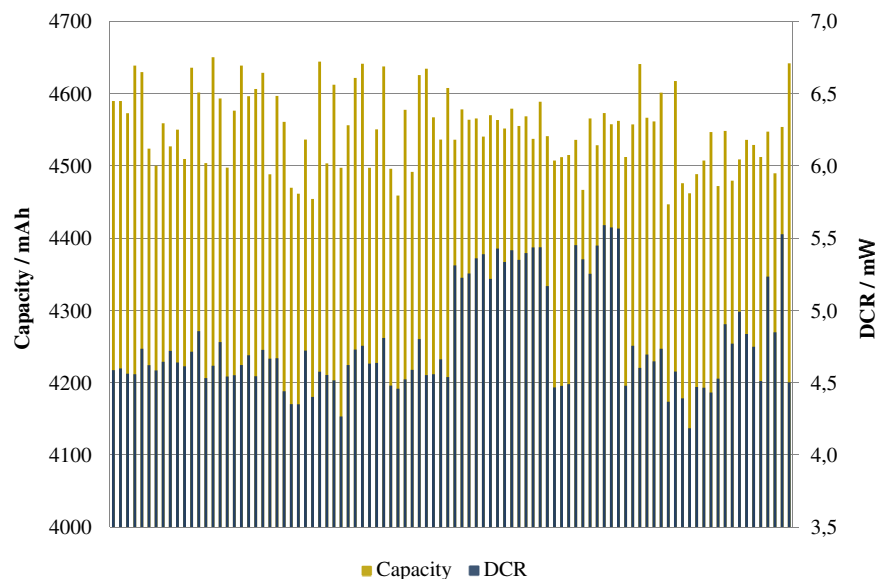

Fig. 11. Measured normalized direct current resistances and initial capacities of all 96 cells in the storage system at begin of life (each bar represents one cell).
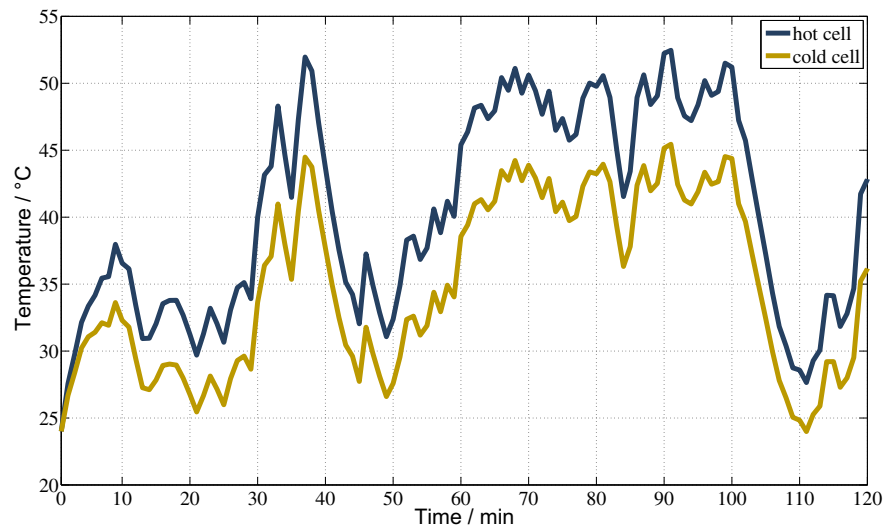
Fig. 12. Simulated temperature development during 2 h of cycling for two cells, comparing highest and lowest cell core temperature in the battery system.
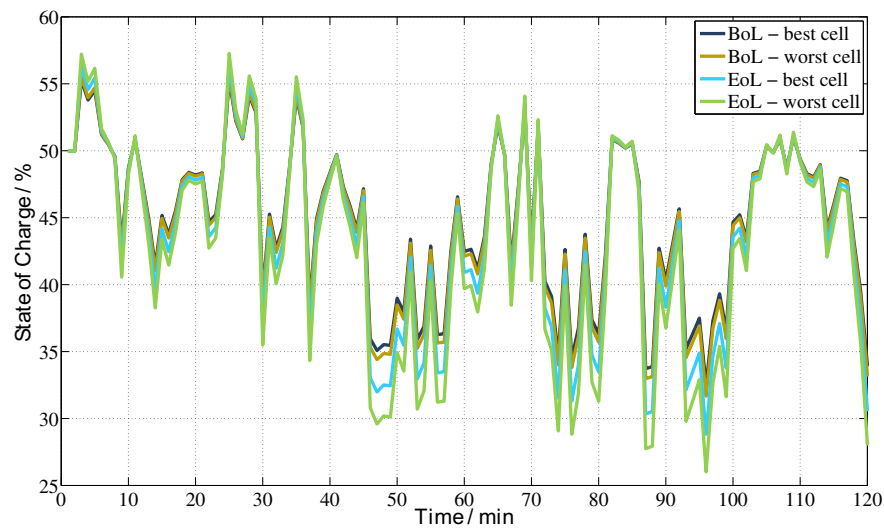

Fig. 13. Simulated SoC development during 2 h of cycling for two cells, comparing highest and lowest cell capacity in the battery system at BoL and end of test (EoL) capacity.
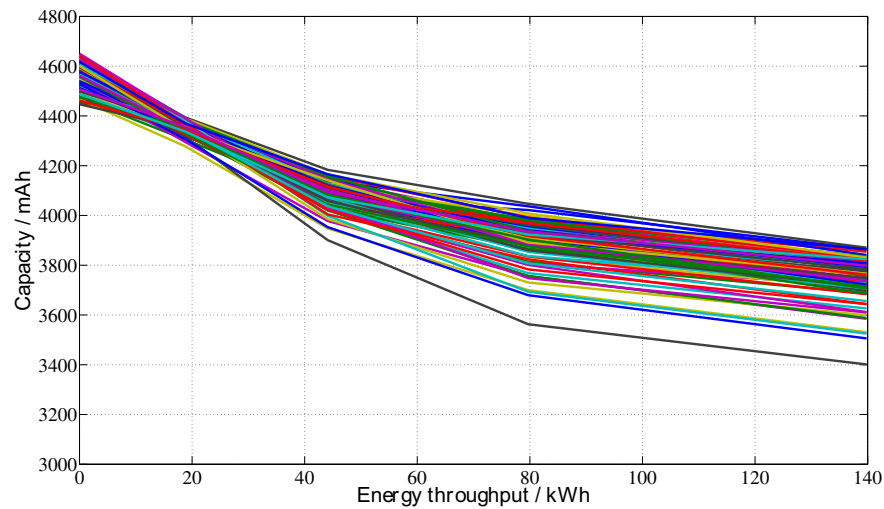

Fig. 14. Measured cell capacity development during cycle life testing. (Each line represents one cell in the battery system).
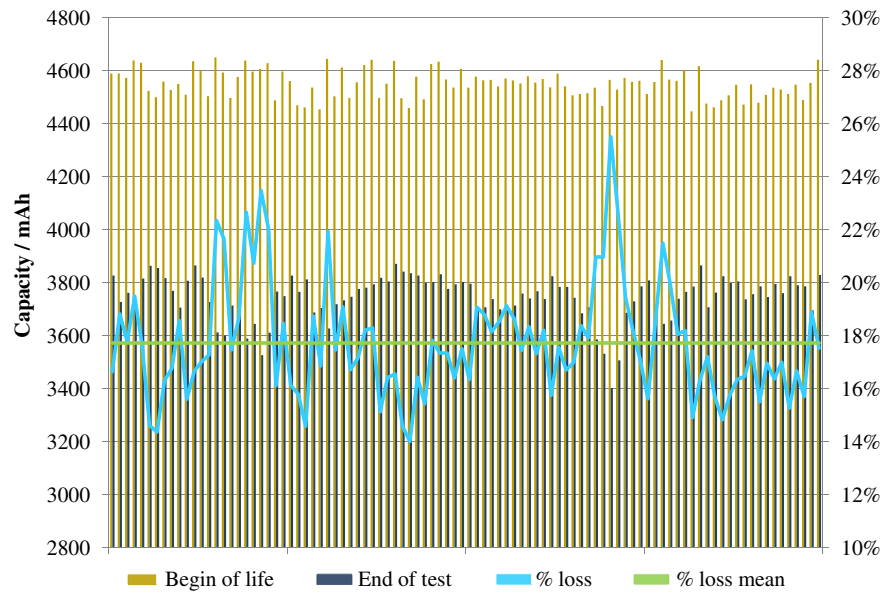
Fig. 15. Measured cell capacities at begin of life (yellow bars) in comparison to the capacities after cycling (black bars); green line: mean capacity loss of all cells; blue line: capacity loss of each cell (refer to the right axis). (Each bar represents one of the 96 cells in the battery system). (For interpretation of the references to colour in this figure legend, the reader is referred to the web version of this article.)

distribution. At this point the measured worst cell has a capacity of approx. 3900 mAh, while the simulated capacity was 3950 mAh. The end of test results shows also a good accordance regarding mean ageing and shape. The marginal area (below 10%) of the simulation at the end of cycling is smaller than in the measurement. A possible reason for this might be the ageing distributions, which are the basis for this simulation. They are based on measurements with a limited number of cells. There might be a bigger ageing spread among all cells.

By using a previous simplified approach, which scales the behaviour of the mean cell to all cells in the entire storage system, the ageing of the battery system is underestimated. Applied to this experiment the mean initial capacity of the cells, and with that the

storage system, would be 4550 mAh (Mean cell @ BoL in Fig. 16). After 45 kWh of cycling the estimated capacity would be 4080 mAh (Mean cell after 45 kWh, Fig. 16). The measured capacity of the worst cell, and with this the storage system, is 3900 mAh. This is an overestimation of battery capacity of approximately 180 mAh, while the outlined simulation approach estimates the capacity with 3950 mAh. Thus, there is a gain in accuracy of more then 100 mAh. After an average capacity loss of 18% during testing the end of test capacity would be 3730 mAh (Mean cell @ End of test). The actual capacity of the storage system, determined by the worst cell, is 3400 mAh (black triangle in Fig. 16). This is an overestimation of the battery capacity of more than 300 mAh. While the outlined approach estimates the end of
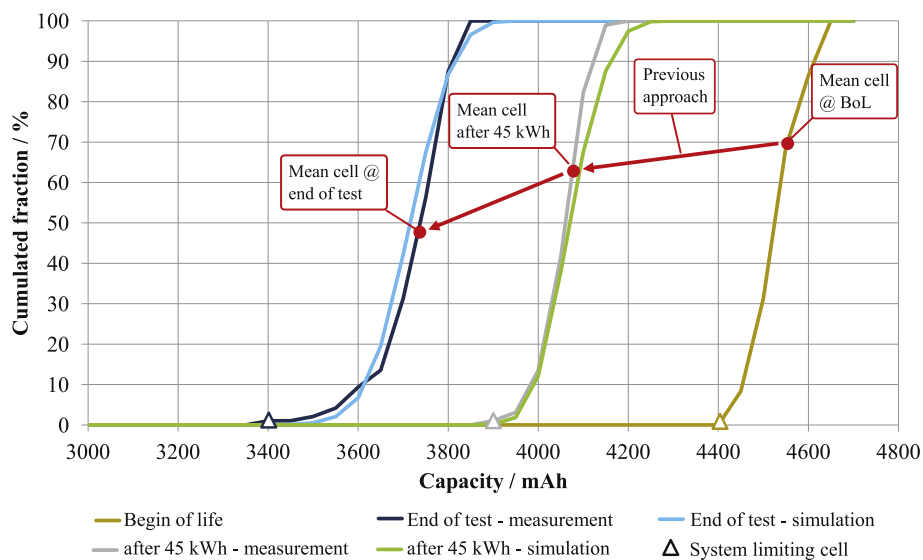

Fig. 16. Cumulated fraction of cell capacities in the battery system at begin of life in comparison to the measured and the simulated capacities after cycling (10 000 simulation trails). Yellow: begin of life; grey: measured after 45 kWh; green: simulated after 45 kWh; black: measured after cycling; blue: simulated after cycling; red: simplified (mean cell) simulation approach. (For interpretation of the references to colour in this figure legend, the reader is referred to the web version of this article.)

test capacity with 3450 mAh. Thus, the consideration of cell-to-cell variation and different thermal condition in the storage system enhance the estimation quality and are hence important for ageing analysis. In summary, cell-to-cell variation and different cell loads due to different thermal condition leads to an inhomogeneous ageing of cells in a storage system.

4. Conclusion

In this article the inhomogeneous ageing of lithium-ion cells, based on LiFePO$_4$-technology, within a storage system was investigated. It provides a simulative approach (involving the Monte Carlo Method) for modelling cell-to-cell variation and different thermal conditions in the storage system and their influence on battery lifetime. The methodology requires a degradation model and spread parameters for calendar and cycle ageing. To show how the method can be applied, an experiment regarding cycle ageing of a battery system was conducted. The results in Fig. 16 show an improvement of estimation accuracy by using the outlined methodology instead of a previous used simplified approach. This previous method, which assumes an identical behaviour of all cells, underestimates the capacity loss of the storage system of roughly 300 mAh, while the outlined approach improves the accuracy up to an underestimation of only 50 mAh. In the experiment the initial capacity spread of the battery system of 200 mAh increases up to 500 mAh at end of testing. This work shows the importance of the consideration of cell-to-cell variation and different thermal conditions in order to investigate battery system ageing, since the worst cell determines the system capacity (cells in series connection).

References

[1] I. Bloom, B. Cole, J. Sohn, S. Jones, E. Polzin, V. Battaglia, G. Henriksen, C. Motloch, R. Richardson, T. Unkelhaeuser, D. Ingersoll, H. Case, Journal of Power Sources 101 (2) (2001) 238–247.
[2] M. Broussely, P. Biensan, F. Bonhommeb, P. Blanchard, S. Herreyre, K. Nechev, R. Staniewicz, Journal of Power Sources 146 (2005) 90–96.
[3] S. Buller, Impedance-based Simulation Models for Energy Storage Devices in Advanced Automotive Power Systems, Ph.D. thesis, RWTH Aachen, 2002.
[4] A. Di Filippi, Stockar, S. Onori, M. Canova, Y. Guezennec, Model-based Life Estimation of Li-ion Batteries in Phevs Using Large Scale Vehicle Simulations: An Introductory Study, in: Vehicle Power and Propulsion Conference (VPPC), 2010, IEEE, 2010.
[5] W. He, N. Williard, M. Osterman, M. Pecht, Journal of Power Sources 196 (23) (2011) 10314–10321.
[6] M. Dubarry, N. Vuillaume, B.Y. Liaw, Journal of Power Sources 186 (2) (2009) 500–507.
[7] M. Fleckenstein, O. Bohlen, M.A. Roscher, B. Bker, Thermal-electrical Inhomogeneities in Li-ion Cells, in: 2nd Technical Conference Advanced Battery Technologies for Automobiles, Mainz (2010).
[8] M. Fleckenstein, O. Bohlen, M.A. Roscher, B. Bker, Journal of Power Sources 196 (10) (2011) 4769–4778.
[9] Z. Li, L. Lu, M. Ouyang, Y. Xiao, Journal of Power Sources 196 (22) (2011) 9757–9766.
[10] G. Ning, R.E. White, B.N. Popov, Electrochimica Acta 51 (2006) 2012–2022.
[11] E. Prada, D.D. Domenico, Y. Creff, J. Bernard, V. Sauvant-Moynot, A Coupled 0d Electrochemical Ageing & Electro-thermal Li-ion Modeling Approach for Hev/Phev, in: Vehicle Power and Propulsion Conference(VPPC), 2011, IEEE, 2011.
[12] R. Spotnitz, J. Franklin, Journal of Power Sources 113 (1) (2003) 81–100.
[13] P. Ramadass, B. Haran, R. White, B.N. Popov, Journal of Power Sources 123 (2) (2003) 230–240.
[14] K. Smith, C.-Y. Wang, Journal of Power Sources 160 (1) (2006) 662–673.